Dynamics of voltage-driven oscillating insulator-metal transitions

Yin Shi, Amy E. Duwel, Dennis M. Callahan, Yifei Sun, F. Anika Hong, Hari Padmanabhan, Venkatraman Gopalan, Roman Engel-Herbert, Shriram Ramanathan, and Long-Qing Chen

Phys. Rev. B **104**, 064308 — Published 19 August 2021

DOI: 10.1103/PhysRevB.104.064308

Dynamics of voltage-driven oscillating insulator-metal transitions

Yin Shi,[1,*] Amy E. Duwel,[2] Dennis M. Callahan,[2] Yifei Sun,[3] F. Anika Hong,[2] Hari Padmanabhan,[1] Venkatraman Gopalan,[1] Roman Engel-Herbert,[1] Shriram Ramanathan,[3] and Long-Qing Chen[1,†]

[1] *Department of Materials Science and Engineering, Materials Research Institute, The Pennsylvania State University, University Park, PA 16802*
[2] *Draper laboratory, Cambridge, MA 02139*
[3] *School of Materials Engineering, Purdue University, West Lafayette, IN 47907*

(Dated: July 20, 2021)

Recent experiments demonstrated emerging alternating insulator and metal phases in Mott insulators actuated by a direct bias voltage, leading to oscillating voltage outputs with characteristic frequencies. Here we develop a physics-based nonequilibrium model to describe the dynamics of oscillating insulator-metal phase transitions and experimentally validate it using a VO_2 device as a prototype. The oscillation frequency is shown to scale monotonically with the bias voltage and series resistance and terminate abruptly at lower and upper device-dependent limits, which are dictated by the nonequilibrium carrier dynamics. We derive an approximate analytical expression for the dependence of the frequency on the device operating parameters, which yields a fundamental limit to the frequency and may be utilized to provide guidance to potential applications of insulator-metal transition materials as building blocks of brain-inspired non-Von Neumann computers.

I. INTRODUCTION

Insulator-metal transitions (IMTs) belong to a large class of phase transitions involving dramatic changes in electronic structures, which are often accompanied by lattice deformations. The vanadium dioxide (VO_2), a strongly correlated system, is perhaps the best studied material that exhibits an IMT [1–4]. Due to the fact that its IMT is near room temperature, VO_2 has been explored for many potential applications such as memristors, sensors, and Mott field-effect transistors [5–9]. Experiments employing a two-terminal VO_2 device with a resistor in series under a direct voltage demonstrated the possible emergence of voltage oscillation across the VO_2 channel resulted from automatic alternation of the insulator and metal phases [10–20]. Such electronic oscillators can emulate neural behavior found in animal brains [21], and the coupling between oscillators leads to synchronization of charge oscillations which can potentially be utilized for non-Boolean computing [22].

There have been a number of theoretical models proposed to describe the voltage oscillation dynamics in VO_2 [23–25]. However, all existing models were based on the assumption that the oscillating phase is kinetically in a quasi-steady state in its instantaneous response to temperature and/or voltage stimuli. The voltage oscillations in these quasi-steady models are purely charging and discharging cycles of a capacitor with their frequencies and oscillation windows defined phenomenologically by the measured switching voltages and on/off resistances. On the other hand, experiments on the voltage-induced IMT in VO_2 revealed that the switching voltages are thermally set by Joule heating [26, 27], but a quasi-steady model incorporating the thermally triggered IMT cannot produce voltage oscillations [23] nonetheless.

Here we report a physics-based nonequilibrium model to describe the dynamics of the IMT and the corresponding voltage oscillation beyond the quasi-steady assumption. In particular, It explicitly incorporates the nonequilibrium dynamics of free charge carriers with a lifetime on the order of 10 μs [28, 29], comparable to periods of possible voltage oscillations. This is important since the free carriers not only determine the device resistance, but also can drive an IMT when their concentration is beyond a critical value [30]. The model yields the correct voltage oscillation characteristics validated by our experiments and still exhibits thermally determined switching voltages as observed in experiments. Importantly, we show that the nonequilibrium carrier dynamics imposes a fundamental limit to the maximal oscillation frequency and identify the physical properties of Mott insulators that will further enhance the maximal frequency. The analysis based on this model and the comparison with experimental measurements clearly demonstrate the key role of the nonequilibrium dynamics of free charge carriers in actuating the voltage oscillation in VO_2.

II. PHYSICS-BASED NONEQUILIBRIUM MODEL

To focus on the dynamics of the oscillating IMT rather than the two-phase morphological patterns, we assume the VO_2 channel of the device to be both homogeneous and charge-neutral during the entire IMT process. We describe the thermodynamic state of VO_2 during the IMT using an electron-correlation order parameter ξ as well as a structural order parameter η with $\xi = 0$ and $\eta = 0$ representing the metallic rutile (R) phase and $\xi \sim -1$ and $\eta \sim 1$ the insulating monoclinic (M1) phase [31–34]. The order parameters evolve to minimize

* yxs187@psu.edu
† lqc3@psu.edu

the total free energy of the system, and for a homogeneous and charge-neutral system, the total free energy density $f(T;\xi,\eta,n)$, where T is the temperature and n is the free electron density. We note that f is referencing to that of the metallic R phase. The free energy density f contains two contributions: the intrinsic bulk free energy density $f_b(T;\xi,\eta)$ and the free energy density of excess free charge carriers $f_{eh}(T;\xi,n)$, i.e., $f = f_b + f_{eh}$ [33, 35–37]. The intrinsic bulk free energy density f_b is approximated by a Landau polynomial with respect to the order parameters [31]. Since the time constants of the relaxation of the order parameters are on the order of picoseconds or less [30, 38] far shorter than the typical voltage oscillation periods in VO_2 oscillators ($\gtrsim 1$ μs), we assume that the order parameters describing the IMT establish equilibrium instantaneously for a given temperature and carrier concentration (considering the temperature and carrier concentration to be independent natural variables), i.e.,

$$\frac{\partial f}{\partial \xi} = \frac{\partial f_b}{\partial \xi} + 2\gamma\xi[n - n_i(T;\xi)] \approx 0, \tag{1}$$

$$\frac{\partial f}{\partial \eta} = \frac{\partial f_b}{\partial \eta} \approx 0, \tag{2}$$

where we have used the relation $\partial f_{eh}/\partial\xi = 2\gamma\xi(n - n_i)$ [33]. $n_i \approx \sqrt{N_c N_v}\exp(-\gamma\xi^2/2k_BT)$ is the intrinsic free carrier density, where k_B is the Boltzmann constant and N_c and N_v are the effective densities of states of the conduction and the valence bands, respectively [33]. Here the energy gap E_g naturally depends on the electronic order parameter and is approximated by $E_g \approx \gamma\xi^2$ where γ is the energy gap of the M1 phase [31–33]. Similar to the thermal driving force $(\partial f_b/\partial\xi, \partial f_b/\partial\eta)$, the term $2\gamma\xi(n - n_i)$ in Eq. (1) is the *electronic* driving force that can reduce the electron correlation (ξ) and induce phase change. This term distinguishes the current model from the existing quasi-steady models [23–25]. Due to this term, for a given temperature [n is subsequently determined by its equation of evolution Eq. (3)], ξ will not be at equilibrium since the resulted n will not necessarily be at equilibrium.

Existing experiments showed that the lifetime of the minority carriers in heavily doped VO_2, τ, is around 10 μs [28, 29], comparable to the typical oscillation periods. We use this value to approximate the VO_2 intrinsic carrier lifetime because to our knowledge there is no other reported measurement of the intrinsic carrier lifetime in the literature. Therefore, it is critical to explicitly incorporate the carrier dynamics in a theoretical model for voltage oscillation. Here we describe the dynamics of free electrons using

$$\frac{\mathrm{d}n}{\mathrm{d}t} = K(n_i^2 - n^2), \tag{3}$$

where $K = 1/2n_r\tau$ is the recombination rate and n_r is a reference electron density.

The temperature evolution in VO_2 subject to a voltage drop V is simply described by the heat equation with a

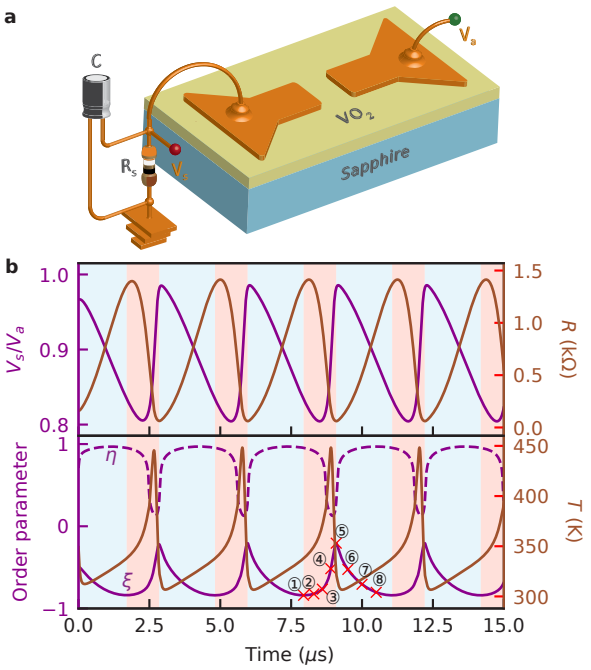

FIG. 1. (a) Schematics of the VO_2 oscillator. V_a is the bias direct voltage, R_s is the series resistor, V_s denotes the voltage drop across the series resistor, and C represents the parasitic capacitance explicitly or it could be an external capacitor. (b) Oscillation patterns of V_s/V_a, the VO_2 resistance R, the order parameters, and the temperature T at $V_a = 7.8$ V and $R_s = 4.7$ kΩ. The light-blue and the light-red shaded regions indicate the processes of the MIT and the IMT, respectively. The numbered red crosses correspond to the phases in Fig. 2(a).

heat source arising from Joule heating,

$$C_v\frac{\mathrm{d}T}{\mathrm{d}t} + \frac{\mathrm{d}u}{\mathrm{d}t} = \frac{V^2}{RL_xL_yL_z} - \frac{h(T - T_s)}{L_z}, \tag{4}$$

where C_v is the heat capacity per unit volume of the metallic R phase, T_s is the ambient temperature, h is the convective heat dissipation coefficient, and u is the internal energy density arising from f. The internal energy density of the metallic R phase can be approximated by C_vT, so $C_vT + u$ constitutes the total internal energy density of VO_2 (f and u are referencing to those of the metallic R phase, respectively). L_x, L_y and L_z are the width, length (in the direction of the electric field), and thickness of the VO_2 channel of a device, respectively. $R = L_y/L_xL_ze\mu n$ is the resistance of the VO_2 channel, where e is the elementary charge and μ is the carrier mobility. Note that R depends on the real-time nonequilibrium density of free electrons n, not the equilibrium density n_i. The $\mathrm{d}u/\mathrm{d}t$ term takes into account the latent heat effect of the first-order IMT [35].

We consider a VO_2 oscillator device schematically depicted in Fig. 1(a). A VO_2 two-terminal device is connected to a direct voltage source V_a through a series resistor R_s. C denotes the parasitic capacitance of the

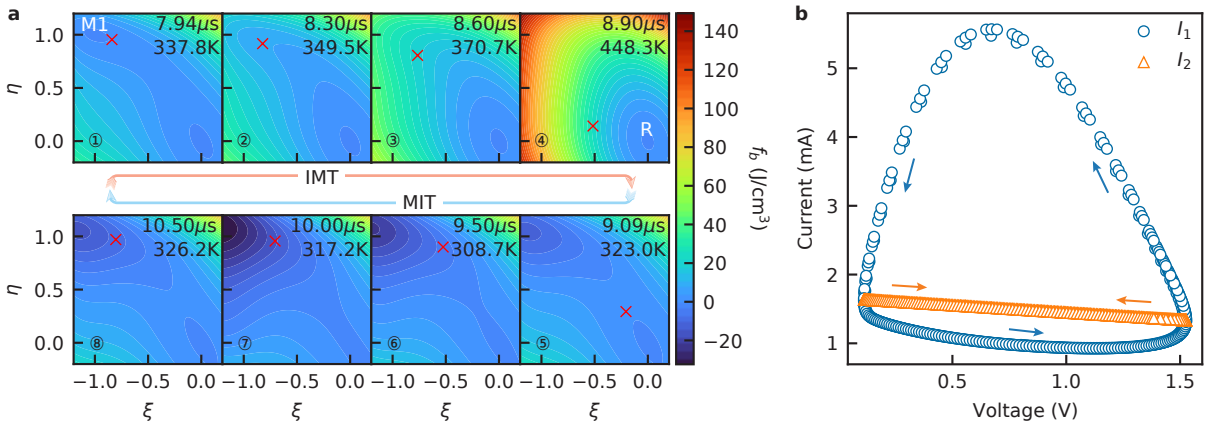

FIG. 2. (a) Phases at a sequence of moments represented by the order parameters superimposed on the intrinsic bulk free energy density landscape for $V_a = 7.8$ V and $R_s = 4.7$ kΩ. The red crosses in (a) correspond to those in Fig. 1(b). The temperature at each moment is shown. The M1 and R minima are marked in ① and ④, respectively. (b) I-V characteristics of VO_2 at $V_a = 7.8$ V and $R_s = 4.7$ kΩ. The x coordinate is the voltage drop across the VO_2 channel. I_1 and I_2 are the current through VO_2 (including the capacitor current) and the current through the resistor (excluding the capacitor current), respectively.

circuit, or an external capacitor that could be added to the circuit. The voltage drop across the series resistor V_s satisfies the Kirchhoff's law, $V = V_a - V_s$ and

$$V_s + R\left(C\frac{\mathrm{d}V_s}{\mathrm{d}t} + \frac{V_s}{R_s}\right) = V_a. \tag{5}$$

If steady states are assumed, the electronic driving force is zero and thus the switching voltage is solely determined by the Joule heating effect, consistent with experiments [26, 27].

Before moving to the simulation results, we analyze some qualitative behaviors that can be predicted by the nonequilibrium model. We expect that the VO_2 resistance, which directly depends on the free electron density n, will not strictly follow the quasi-steady resistance determined by the VO_2 temperature. This is clear from Eq. (3), which indicates that n will lag behind n_i. The time constant for the temperature evolution $C_v L_z/h$ will be far shorter than the voltage oscillation periods for thin films (small L_z and large h). In this case, Eq. (4) corresponds to quasi-steady states and the voltage oscillation period is determined by the free electron lifetime and the RC time constant. The oscillation period will be longer for longer free electron lifetimes and larger R_sC values.

III. NONEQUILIBRIUM CHARACTERISTICS OF OSCILLATING IMTS

In our experiments, the two-terminal device in Fig. 1(a) employs a VO_2 thin film grown on a sapphire substrate, and is supplied with a direct voltage with a resistor in series [35]. The parameters used for modeling the device characteristics by simultaneously solving Eqs. (1-5) are the same as those in experiments [35]. Figure 1(b) shows the calculated oscillation patterns of various variables at $V_a = 7.8$ V and $R_s = 4.7$ kΩ. The processes of the metal-insulator transition (MIT, marked as light blue) and the IMT (marked as light red) are identified by falling and rising parts of the ξ pattern, respectively. The voltage drop across the series resistor has an oscillation amplitude around 18% of the bias voltage. It rises quickly and falls relatively slowly with a ratio of the rise and fall times of 0.26 and transits from rise to fall smoothly, consistent with experiments [10, 11, 22]. $|\xi|$ and $|\eta|$ never reach exactly 0 and 1, indicating that VO_2 is never in the fully metallic or fully insulating state. The peaks of ξ and the troughs of R have a delay of 0.19 μs to the peaks of temperature, meaning that the VO_2 channel at the highest temperature is actually not the most metallic, which is a clear evidence of the non-instantaneous response of the electronic phase to temperature. The temperature reaches 450 K consistent with the experiment [16]. The peaks of ξ also have a short delay to the troughs of η. Furthermore, the peaks of R have a delay of 0.19 μs to the troughs of ξ, revealing that the VO_2 resistance has a finite response time to the electronic phase.

Next we examine the evolution of the phase and the free energy landscape during the oscillation [Fig. 2(a)]. From a trough of the ξ pattern to its trailing peak [red crosses in Fig. 1(b)], the phase evolves from the vicinity of the M1 minimum of f_b to the vicinity of the saddle point. From the peak to the next trough, the phase returns to the vicinity of the M1 minimum yet following a different route from the pathway on which it appears. The phase never resides exactly at the minimum or the saddle point of f_b, indicating that during the oscillation the state is always transient. The non-steady phase trajectory corresponds to non-steady flows in the I-V plane as shown in Fig. 2(b). Both the current through VO_2 (I_1) and

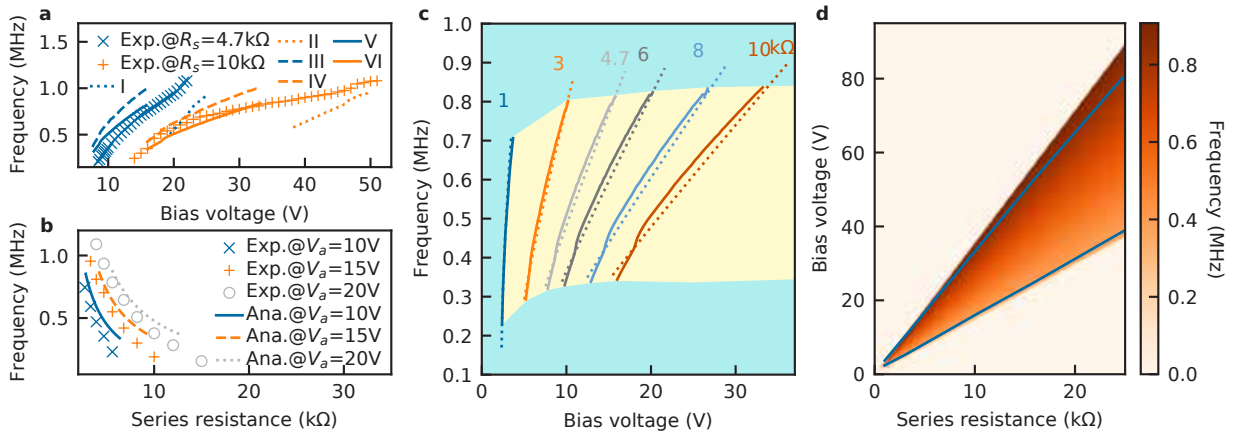

FIG. 3. (a) Experimentally measured (markers) and simulated (lines) frequency scaling with the bias voltage V_a at $R_s = 4.7$ kΩ and 10 kΩ. The scaling calculated with different τ and C is shown. I: $R_s = 4.7$ kΩ, $\tau = 7$ μs, $C = 250$ pF; II: $R_s = 10$ kΩ, $\tau = 7$ μs, $C = 250$ pF; III: $R_s = 4.7$ kΩ, $\tau = 11$ μs, $C = 550$ pF; IV: $R_s = 10$ kΩ, $\tau = 11$ μs, $C = 550$ pF; V: $R_s = 4.7$ kΩ, $\tau = 14$ μs, $C = 700$ pF; VI: $R_s = 10$ kΩ, $\tau = 14$ μs, $C = 700$ pF. (b) Experimentally measured (markers) and analytical (lines) frequency scaling with R_s at different V_a. (c) Numerically simulated (solid lines) and analytical (dotted lines) frequency scaling with V_a at various R_s. The colored numbers indicate the corresponding R_s values in units of kiloohm. The light yellow and light blue shades mark the regions of oscillation and no oscillation, respectively. (d) Numerically simulated (solid lines) boundaries of the range of oscillation superimposed on the frequency map over the bias voltage and series resistance obtained by the analytical formulae.

the current through the series resistor (I_2) possess the negative differential resistance (NDR) with non-steady intermediate NDR states. In contrast, a quasi-steady model [23–25] is not possible to access the non-steady intermediate states that connect the fully metallic and fully insulating states.

We then study the oscillation frequency scaling with the bias voltage and series resistance. The calculations show that the frequency increases monotonically as the voltage increases [Fig. 3(a)]. As V_a increases, the oscillation suddenly emerges at a finite low bias and then gets overdamped at a high bias, which mark the low and high bias limits on the calculated frequency scaling curves. Indeed, VO_2 remains in the M1 phase for sufficiently low voltages and is excited permanently to the R phase for sufficiently high voltages. These are all consistent with our experimental results. The simulations also reveal that larger τ and C reduce the slopes of the frequency scaling curves and shift the curves to lower bias. For $\tau = 14$ μs and $C = 700$ pF [35], the calculated frequency scaling curves are in very good agreement with the experimentally measured ones. Some discrepancies in the V_a range of oscillation may be attributed to the homogeneity assumption such that the nucleation temperature of the M1 phase in the homogeneous R phase is lower than that in the realistic inhomogeneous VO_2 samples. The lower the M1 nucleation temperature is, the lower the upper voltage limit for oscillation, because for bias voltages higher than the upper voltage limit the temperature will stay high so that the M1 phase cannot nucleate and the voltage oscillation ceases. Therefore, the upper voltage limit for oscillation calculated for the homogeneous VO_2 is lower than that measured for the generally inhomogeneous sample. The homogeneity assumption is not expected to significantly affect other observed quantities, because we already used in the simulations the experimentally measured resistances, free carrier lifetime, etc.. Figure 3(c) presents the calculated full frequency scaling with V_a at various R_s, whose slope decreases with increasing R_s.

IV. ANALYTICAL FORMULAE AND FUNDAMENTAL LIMIT FOR OSCILLATION FREQUENCY

To better understand and engineer the Mott electronic oscillators, we derive approximate analytical expressions for the angular frequency ω and range of oscillation by linearizing Eqs. (1-5) around the superheating state [35],

$$\omega^2 \approx \frac{\alpha V_a^2 Q(Q+1)}{4G_{th}CR_s^2},\ Q = \sqrt{1 - \frac{4G_{th}\Delta T R_s}{V_a^2}}, \quad (6)$$

$$v(R_s) < V_a < 1.71\sqrt{\alpha G_{th} C}\Delta T R_s - 0.121\sqrt{\frac{G_{th}}{\alpha C}}, \quad (7)$$

$$R_s > \frac{1.51}{\alpha C \Delta T}, \quad (8)$$

with $v(R_s)$ being a branched function of R_s,

$$v(R_s) \approx \begin{cases} 2\sqrt{G_{th}\Delta T R_s}, & R_s < \dfrac{4}{\alpha C \Delta T}, \\ \sqrt{\dfrac{\alpha C G_{th}}{2}}\Delta T R_s + \sqrt{\dfrac{G_{th}}{2\alpha C}}, & R_s > \dfrac{4}{\alpha C \Delta T}. \end{cases}$$

Here $\alpha = \beta k_B/\gamma\tau$ is a parameter dependent only on intrinsic properties of VO_2, where β is a dimensionless

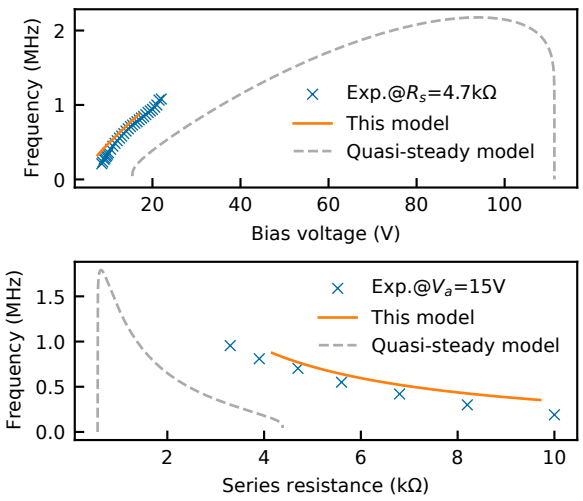

FIG. 4. Comparison of the experimentally measured frequency scaling (crosses) and the analytical frequency formulae derived from this model (solid lines) and the quasi-steady model (dashed lines). The upper panel is for the scaling with V_a at $R_s = 4.7$ kΩ and the lower panel is for the scaling with R_s at $V_a = 15$ V.

material-specific constant. $\Delta T = T_{sh} - T_s$ where T_{sh} is the superheating temperature. $G_{th} = L_x L_y h$ is the effective thermal conductance of the device.

Figure 3(b,c) shows the oscillation behaviors predicted by the analytical formulae Eqs. (6-8), which match well with the experimental and simulation results. For fixed V_a, R_s, and C, the frequency increases as the ambient temperature T_s increases, in agreement with experimental measurements [12]. The calculated R_s range of oscillation is narrower than the measured one, similar to the case of V_a range of oscillation for the same reason. We further use the analytical formulae to generate the frequency map over the bias voltage and series resistance and plot it together with the numerically simulated ranges of voltage oscillation [Fig. 3(d)]. The region of oscillation has a shape of a sector, in excellent agreement with the experiment [10]. It terminates at around $R_s = 1$ kΩ yet extends to infinite R_s.

To understand the important role of the nonequilibrium dynamics of free charge carriers in the voltage oscillation, we compare the frequency scaling from the experimental measurements, our nonequilibrium model, and the quasi-steady model [24, 35] in Fig. 4. The frequency scaling from the quasi-steady model is qualitatively different from the experimentally measured ones yet with large quantitative deviations. In contrast, both the magnitudes of the frequencies and the dependence of the frequency on the bias voltage and series resistance obtained from our nonequilibrium model show remarkably good agreement with our experimental results, demonstrating the critical role of the nonequilibrium charge carrier dynamics in the voltage oscillation.

The nonequilibrium carrier dynamics also imposes a fundamental limit to the maximal frequency achievable in a VO_2 oscillator. This is contrary to the previous understanding that the oscillation frequency will go arbitrarily high as the RC time constant and the heat-dissipation time constant approach zero. Indeed, the slow internal carrier dynamics will dominate the oscillation process when the external charging/discharging and heating/cooling dynamics become sufficiently fast. Using Eqs. (6-8), we can project the maximal frequency limit of a VO_2 oscillator [35],

$$\nu_M \approx 0.193 \alpha T_{sh} = 7 \text{ MHz}. \tag{9}$$

ν_M is a fundamental limit to the frequency, i.e., it only depends on the intrinsic parameters of the material. To approach the maximal frequency limit, one needs to lower the ambient temperature, increase the series resistance, and then tune up the voltage to the high bias limit of oscillation. The ability to shift the resonance frequency dynamically makes VO_2 attractive for forming oscillator arrays [22]. Equation (9) also provides guidance on searching for new IMT materials that could form electronic oscillators with gigahertz oscillation frequencies, that is, materials with short carrier lifetimes and small energy gaps in their insulating phases.

V. CONCLUSIONS

We presented a nonequilibrium model to predict and understand the dynamics of oscillating IMTs in Mott insulators and experimentally validated it by measuring the voltage oscillation in a two-terminal VO_2 oscillator. The nonequilibrium dynamics of free charge carriers is critical for generating the experimentally observed oscillation behavior, unambiguously demonstrating that the phase transition during the voltage oscillation is partially electronically driven. Such nonequilibrium carrier dynamics may be the missing dynamics in understanding the chaotic voltage oscillation observed in another Mott insulator NbO_2 [39]. We also derived approximate expressions for the oscillation frequency scaling and range of oscillation, revealing that the nonequilibrium carrier dynamics imposes a fundamental limit to the maximal frequency. Subsequently the material property parameters that can enhance the fundamental frequency limit are clearly identified. This physics-based model offers a foundation for future studies of the dynamics of oscillating IMTs and provides guidance on designing high-frequency electronic oscillator devices based on IMT materials.

ACKNOWLEDGMENTS

The theoretical and computational effort of this work was supported as part of the Computational Materials

Sciences Program funded by the U.S. Department of Energy, Office of Sciences, Basic Energy Sciences, under Award No. DE-SC0020145. The experimental effort on oscillator devices was supported by ONR N00014-16-1-2398.

[1] F. J. Morin, Oxides Which Show a Metal-to-Insulator Transition at the Neel Temperature, Phys. Rev. Lett. **3**, 34 (1959).

[2] S. Biermann, A. Poteryaev, A. I. Lichtenstein, and A. Georges, Dynamical Singlets and Correlation-Assisted Peierls Transition in VO_2, Phys. Rev. Lett. **94**, 026404 (2005).

[3] H. Zheng and L. K. Wagner, Computation of the Correlated Metal-Insulator Transition in Vanadium Dioxide from First Principles, Phys. Rev. Lett. **114**, 176401 (2015).

[4] W. H. Brito, M. C. O. Aguiar, K. Haule, and G. Kotliar, Metal-Insulator Transition in VO_2: A DFT+DMFT Perspective, Phys. Rev. Lett. **117**, 056402 (2016).

[5] F. Liao, Z. Zhu, Z. Yan, G. Yao, Z. Huang, M. Gao, T. Pan, Y. Zhang, Q. Li, X. Feng, and Y. Lin, Ultrafast response flexible breath sensor based on vanadium dioxide, Journal of Breath Research **11**, 036002 (2017).

[6] M. Nakano, K. Shibuya, D. Okuyama, T. Hatano, S. Ono, M. Kawasaki, Y. Iwasa, and Y. Tokura, Collective bulk carrier delocalization driven by electrostatic surface charge accumulation, Nature **487**, 459 (2012).

[7] M. Son, J. Lee, J. Park, J. Shin, G. Choi, S. Jung, W. Lee, S. Kim, S. Park, and H. Hwang, Excellent Selector Characteristics of Nanoscale VO2 for High-Density Bipolar ReRAM Applications, Electron Device Letters, IEEE **32**, 1579 (2011).

[8] T. Driscoll, H.-T. Kim, B.-G. Chae, M. Di Ventra, and D. N. Basov, Phase-transition driven memristive system, Applied Physics Letters **95**, 043503 (2009).

[9] Z. Yang, C. Ko, and S. Ramanathan, Oxide Electronics Utilizing Ultrafast Metal-Insulator Transitions, Annual Review of Materials Research **41**, 337 (2011).

[10] Y. W. Lee, B.-J. Kim, J.-W. Lim, S. J. Yun, S. Choi, B.-G. Chae, G. Kim, and H.-T. Kim, Metal-insulator transition-induced electrical oscillation in vanadium dioxide thin film, Applied Physics Letters **92**, 162903 (2008).

[11] H.-T. Kim, B.-J. Kim, S. Choi, B.-G. Chae, Y. W. Lee, T. Driscoll, M. M. Qazilbash, and D. N. Basov, Electrical oscillations induced by the metal-insulator transition in vo2, Journal of Applied Physics **107**, 023702 (2010).

[12] M. Pattanayak, M. N. F. Hoque, Y. Zhao, Z. Fan, and A. A. Bernussi, Tunable VO2 relaxation oscillators for analog applications, Semiconductor Science and Technology **34**, 105028 (2019).

[13] J. Sakai, High-efficiency voltage oscillation in vo2 planer-type junctions with infinite negative differential resistance, Journal of Applied Physics **103**, 103708 (2008), https://doi.org/10.1063/1.2930959.

[14] Y. Wang, J. Chai, S. Wang, L. Qi, Y. Yang, Y. Xu, H. Tanaka, and Y. Wu, Electrical oscillation in pt/vo2 bilayer strips, Journal of Applied Physics **117**, 064502 (2015), https://doi.org/10.1063/1.4907906.

[15] D. Lepage and M. Chaker, Thermodynamics of self-oscillations in vo2 for spiking solid-state neurons, AIP Advances **7**, 055203 (2017), https://doi.org/10.1063/1.4983175.

[16] S. G. Bortnikov, V. S. Aliev, I. A. Badmaeva, and I. V. Mzhelskiy, Vo2 film temperature dynamics at low-frequency current self-oscillations, Journal of Applied Physics **123**, 075701 (2018), https://doi.org/10.1063/1.5010971.

[17] A. Velichko, M. Belyaev, V. Putrolaynen, V. Perminov, and A. Pergament, Modeling of thermal coupling in vo2-based oscillatory neural networks, Solid-State Electronics **139**, 8 (2018).

[18] A. Velichko, M. Belyaev, V. Putrolaynen, V. Perminov, and A. Pergament, Thermal coupling and effect of subharmonic synchronization in a system of two vo2 based oscillators, Solid-State Electronics **141**, 40 (2018).

[19] E. Corti, B. Gotsmann, K. Moselund, A. M. Ionescu, J. Robertson, and S. Karg, Scaled resistively-coupled vo2 oscillators for neuromorphic computing, Solid-State Electronics **168**, 107729 (2020), special Issue of Solid-State Electronics, dedicated to EUROSOI-ULIS 2019.

[20] R. Tobe, M. S. Mian, and K. Okimura, Coupled oscillations of vo2-based layered structures: Experiment and simulation approach, Journal of Applied Physics **127**, 195103 (2020), https://doi.org/10.1063/5.0001382.

[21] J. Lin, S. Guha, and S. Ramanathan, Vanadium dioxide circuits emulate neurological disorders, Frontiers in Neuroscience **12**, 856 (2018).

[22] N. Shukla, A. Parihar, E. Freeman, H. Paik, G. Stone, V. Narayanan, H. Wen, Z. Cai, V. Gopalan, R. Engel-Herbert, *et al.*, Synchronized charge oscillations in correlated electron systems, Scientific reports **4**, 4964 (2014).

[23] T. Driscoll, J. Quinn, M. Di Ventra, D. N. Basov, G. Seo, Y.-W. Lee, H.-T. Kim, and D. R. Smith, Current oscillations in vanadium dioxide: Evidence for electrically triggered percolation avalanches, Phys. Rev. B **86**, 094203 (2012).

[24] P. Maffezzoni, L. Daniel, N. Shukla, S. Datta, and A. Raychowdhury, Modeling and simulation of vanadium dioxide relaxation oscillators, IEEE Transactions on Circuits and Systems I: Regular Papers **62**, 2207 (2015).

[25] A. Parihar, N. Shukla, S. Datta, and A. Raychowdhury, Synchronization of pairwise-coupled, identical, relaxation oscillators based on metal-insulator phase transition devices: A model study, Journal of Applied Physics **117**, 054902 (2015).

[26] S. B. Lee, K. Kim, J. S. Oh, B. Kahng, and J. S. Lee, Origin of variation in switching voltages in threshold-switching phenomena of VO2 thin films, Applied Physics Letters **102**, 063501 (2013).

[27] A. Zimmers, L. Aigouy, M. Mortier, A. Sharoni, S. Wang, K. G. West, J. G. Ramirez, and I. K. Schuller, Role of Thermal Heating on the Voltage Induced Insulator-Metal Transition in VO_2, Phys. Rev. Lett. **110**, 056601 (2013).

[28] C. Miller, M. Triplett, J. Lammatao, J. Suh, D. Fu, J. Wu, and D. Yu, Unusually long free carrier lifetime and metal-insulator band offset in vanadium dioxide, Phys. Rev. B **85**, 085111 (2012).

[29] Y. Zhou and S. Ramanathan, Gan/vo2 heteroepitaxial p-n junctions: Band offset and minority carrier dynamics, Journal of Applied Physics **113**, 213703 (2013).
[30] D. Wegkamp, M. Herzog, L. Xian, M. Gatti, P. Cudazzo, C. L. McGahan, R. E. Marvel, R. F. Haglund, A. Rubio, M. Wolf, and J. Stähler, Instantaneous Band Gap Collapse in Photoexcited Monoclinic VO_2 due to Photocarrier Doping, Phys. Rev. Lett. **113**, 216401 (2014).
[31] Y. Shi, F. Xue, and L.-Q. Chen, Ginzburg-Landau theory of metal-insulator transition in VO 2 : The electronic degrees of freedom, Europhysics Letters **120**, 46003 (2017).
[32] Y. Shi and L.-Q. Chen, Phase-field model of insulator-to-metal transition in VO_2 under an electric field, Phys. Rev. Materials **2**, 053803 (2018).
[33] Y. Shi and L.-Q. Chen, Current-driven insulator-to-metal transition in strongly correlated vo_2, Phys. Rev. Applied **11**, 014059 (2019).
[34] Y. Shi and L.-Q. Chen, Spinodal electronic phase separation during insulator-metal transitions, Phys. Rev. B **102**, 195101 (2020).
[35] See Supplemental Material for detailed descriptions of the free energy density of excess free charge carriers, the internal energy density, the experiment and simulation setup, the quasi-steady model, and the derivation of the analytical frequency formulae, which includes Refs. [36, 37].
[36] A. N. Morozovska, E. A. Eliseev, O. V. Varenyk, Y. Kim, E. Strelcov, A. Tselev, N. V. Morozovsky, and S. V. Kalinin, Nonlinear space charge dynamics in mixed ionic-electronic conductors: Resistive switching and ferroelectric-like hysteresis of electromechanical response, Journal of Applied Physics **116**, 066808 (2014).
[37] J. H. Park, J. M. Coy, T. S. Kasirga, C. Huang, Z. Fei, S. Hunter, and D. H. Cobden, Measurement of a solid-state triple point at the metal-insulator transition in VO2, Nature **500**, 431 (2013).
[38] A. Cavalleri, C. Tóth, C. W. Siders, J. A. Squier, F. Ráksi, P. Forget, and J. C. Kieffer, Femtosecond Structural Dynamics in VO_2 during an Ultrafast Solid-Solid Phase Transition, Phys. Rev. Lett. **87**, 237401 (2001).
[39] S. Kumar, J. P. Strachan, and R. S. Williams, Chaotic dynamics in nanoscale nbo 2 mott memristors for analogue computing, Nature **548**, 318 (2017).